1617 nm emission control of an Er:YAG laser by a corrugated single-layer resonant grating mirror

Adrien Aubourg, Martin Rumpel, Julien Didierjean, Nicolas Aubry, Thomas Graf, François Balembois, Patrick Georges, Marwan Abdou Ahmed

1617 nm emission control of an Er:YAG laser by a corrugated single-layer resonant grating mirror

Adrien Aubourg,[1,2,*] **Martin Rumpel,**[3] **Julien Didierjean,**[2] **Nicolas Aubry,**[2] **Thomas Graf,**[3]
François Balembois,[1] **Patrick Georges,**[1] **and Marwan Abdou Ahmed**[3]

[1]*Laboratoire Charles Fabry, Institut d'Optique, CNRS, Université Paris-Sud—2 Av A.Fresnel, 91127 Palaiseau Cedex, France*

[2]*Fibercryst—La Doua, Bat. l'Atrium, Bd Latarjet, F-69616 Villeurbanne, France*

[3]*Institut für Strahlwerkzeuge (IFSW), Universität Stuttgart, Pfaffenwaldring 43, 70569 Stuttgart, Germany*

*Corresponding author: adrien.aubourg@institutoptique.fr

A resonant grating mirror (RGM) that combines a single layer planar waveguide and a subwavelength grating is used to simultaneously control the beam quality, the spectral bandwidth, and the polarization state of an Er:YAG laser. This simple device is compared to classical methods using several intracavity components: an etalon for wavelength selection, a thin film polarizer for polarization selection, and an aperture for spatial filtering. It is demonstrated that the RGM provides the same polarization purity, an enhanced spectral filtering, and a significant improvement of the beam quality. In CW operation, the Er:YAG laser with a RGM emits an output power of 1.4 W at 1617 nm with a M^2 of 1.4.

Resonantly diode-pumped Er:YAG laser cavities are studied for their capability to emit a laser beam at wavelengths within the eye-safe region, i.e., at 1617 and 1645 nm, where the atmosphere is mostly transparent. The natural laser emission (i.e., without any wavelength selective component in the cavity) of Er:YAG occurs at 1645 nm since it requires a lower population inversion. However, for applications requiring kilometer range propagation such as telemetry, wind mapping, active imaging, or Lidar in general, laser operation at 1617 nm is more efficient since the atmosphere is free of methane absorption at this wavelength [1]. Moreover, polarized emission is useful for the detection of atmosphere pollutants or materials. Finally, a high beam quality ($M^2 \sim 1$) is required to improve the effective range of the detection device [1].

One possible way to achieve wavelength, polarization, and beam quality control of the laser emission is to use intracavity components such as etalons, polarizers, and hard apertures (e.g., pinholes). This solution, however, uses three different optical components. Ideally, one component providing these three functions would simplify the cavity design. A resonant grating mirror (RGM) [2] can potentially fulfil these requirements. A RGM results from the combination of a planar waveguide (single or multilayer) and a subwavelength diffraction grating. This leads to resonances in transmission or reflection [3–5] for a given wavelength, angle of incidence (AOI), and polarization state of the incident beam. The basic principle of the resonant behavior of a RGM is related to the excitation of a guided mode in the waveguide, together with destructive interferences in transmission in the present case. Hence, all energy is reflected with a theoretical efficiency of 100%.

RGMs were already used to polarize and tune the wavelength of a Yb:YAG thin-disk laser at very high output powers [2,6,7].

In this Letter, we study for the first time, to the best our knowledge, the potential of RGM for emission control of an Er:YAG laser including wavelength selection, polarization control, and spatial filtering.

The RGM structure used in this work is composed of a fused silica substrate ($n = 1.45$), a single-layer Ta_2O_5 waveguide ($n = 2.15$), and a subwavelength grating, as depicted in Fig. 1(a). The binary grating structure with a nominal grating period of 700 nm, a groove depth of 50 nm and a duty cycle of 50% is first etched into the substrate by means of standard interference beam lithography, followed by a reactive ion etching process. In a further step, the 500 nm thick coating layer forming the waveguide is then deposited by means of ion beam sputtering (IBS) technology. In Fig. 1(b), an atomic force microscope (AFM) scan of the fabricated RGM is shown.

At 1617 nm and for TE polarization we calculated a guided-mode resonance at an AOI of 24.43°. The calculated reflectivity at 1617 nm is $R_{TE} = 99.99\%$ for TE polarization and approximately 16% for TM polarization. Figure 2 shows the calculated reflectivities versus wavelength of the above described structure for both polarization states.

Further simulations have been performed in order to study the spectral bandwidth (full width half-maximum, FWHM) of the resonance peak at different AOI. Figure 3 shows the obtained results for AOI ranging from 22.5° to 25.5° and for the same grating and waveguide parameters
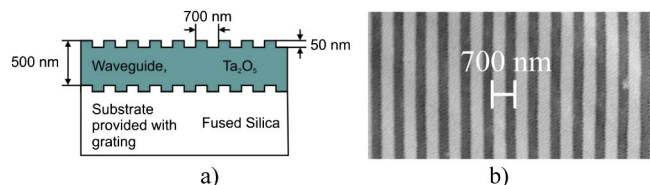

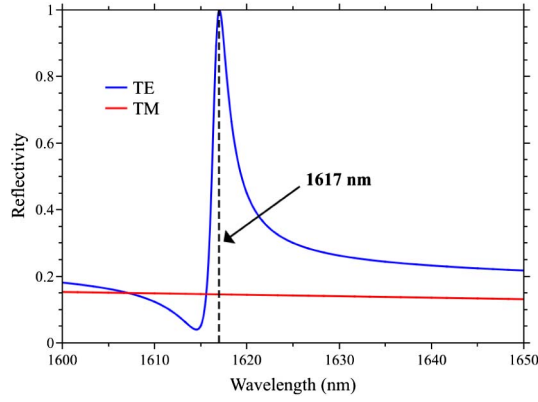Fig. 1.   (a) RGM structure and (b) AFM scan of the surface.

Fig. 2. Calculated reflectivity versus the wavelength for TE and TM polarization at an AOI of 24.43° around 1617 nm.

Fig. 4. Characterization setup.

(groove depth, duty cycle, period, and thickness). As can be seen, an increase of 0.4 nm of the spectral bandwidth is observed over the above AOI (corresponding to a wavelength range between 1600 and 1630 nm). Within the spectral range of interest, i.e., 1615–1620 nm, the FWHM increase is very minor and amounts to only 0.07 nm. The calculated reflectivities for TE polarization at 24.18°, 23.43°, and 24.93° are also shown in Fig. 3 to illustrate the minor change in the resonance peaks.

After its production and in order to precisely identify the AOI at which the resonance occurs for the 1617 nm wavelength, the RGM was introduced in the spectroscopic characterization bench depicted in Fig. 4. It combines a fiber-coupled diode laser emitting at around 1617 nm and a polarizing beam splitter with an extinction ratio of 1000:1 to subsequently polarize the beam after collimation. The RGM itself was mounted to an automated high-precision rotary stage (with a resolution of 0.01°). A photodiode is coupled to the setup to measure the transmitted power of the beam for every AOI.

Figure 5 reports on the measured angular spectra. A discrepancy in the resonance from 24.43° to 24.18° (+0.25°) was found from the spectroscopic characterization. Moreover, the exact grating period was measured optically, using the Littrow configuration, to be 703.2 nm instead of 700 nm. These two results can be attributed to manufacturing tolerances (including refractive index and thickness of the waveguide as well as grating groove depth). This can be attributed to manufacturing tolerances. A maximum reflectivity of around 97% is extracted
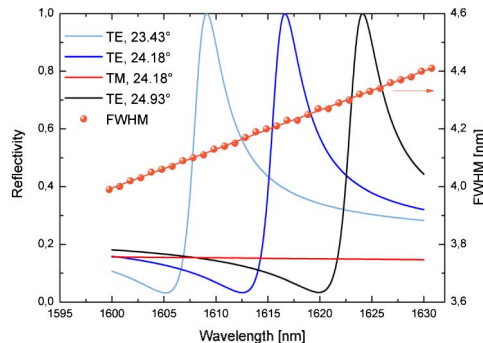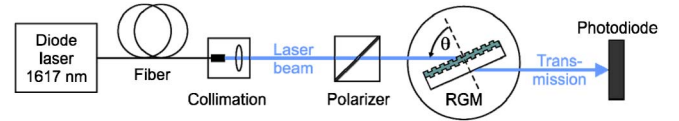
from the measured transmission. Two effects can explain this low value compared to the theoretical one (99.99%). First, the imperfectly collimated beam used in our experimental setup is known to affect the amplitude of the resonance peak as well as its spectral/angular bandwidth [5]. Second, absorption in the waveguide and scattering losses can also reduce the reflectivity value. Simulation iterations were performed in order to match the measured and the calculated spectra as shown in Fig. 5. A good overlap for the peak reflectivity was achieved by increasing the grating depth from 50 to 70 nm, as already suggested by our AFM measurements.

This characterization showed that the RGM provides a unique combination of polarization selectivity, spectral selectivity (Fig. 2), and angular selectivity (Fig. 5). In order to demonstrate its potential, we designed and built the diode-pumped Er:YAG lasers depicted in Figs. 6(a) and 6(b) to provide a comparative study between classical methods of laser emission control [including a thin-film polarizer (TFP), an etalon, and an aperture] and the emission control by the RGM. These cavities are designed to provide a large beam waist diameter (1.6 mm) with a small divergence. Hence, the RGM reflectivity will be close to its maximum. The laser beam will fulfil the coupling (guided-mode excitation) condition of the mirror, giving rise to the resonance effect [8].

The lasers are 400 mm long and are composed of a dichroic [highly transmissive (HT) at 1532 nm and highly reflective (HR) at 1617–1645 nm] meniscus (M1) with a radius of curvature (ROC) of 100 mm, a highly reflective mirror (M2) with a ROC of 400 mm to collimate the beam, and a plane output coupler (M3) with a transmission of 20% around 1.6 μm. The collimation of the laser beam is done by moving the furthest possible mirror M3 with full pump power without shutting the laser off. Thanks to the low quantum defect, the focal length of the thermal length is around 400 mm at maximum pump power. With this setup, the laser beam waist has a diameter of 350 μm and is located inside the crystal. We did not observe a

Fig. 3. Calculated reflectivity and FWHM versus the wavelength at different AOI for TE and TM polarization.
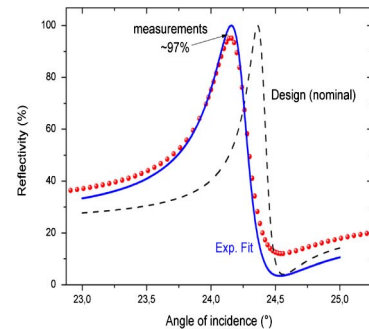

Fig. 5. Measured (red dotted line) and calculated (blue solid line) TE reflectivity versus AOI of the RGM. The fit corresponds to an adjustment of the theoretical reflectivity without scattering-, absorption-, or divergence-related losses.
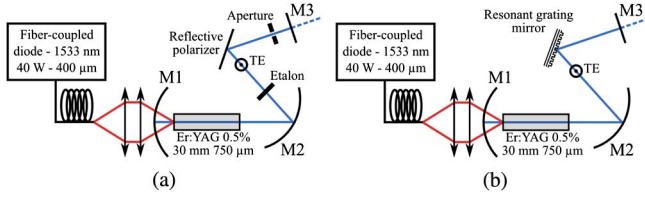
Fig. 6. (a) Resonator setup with thin film polarizer, an etalon, and an aperture. The beam is collimated between M2 and M3 mirrors. The etalon ensures wavelength selectivity (from 1645 to 1617 nm) and the polarizer ensures linear vertical polarized output. The aperture reduces the power contributions of higher order Gaussian modes. (b) The resonator setup with the RGM.
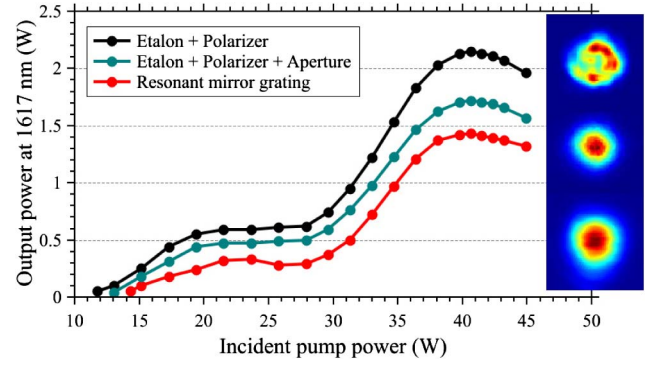

Fig. 7. Efficiency curves for the three setups with their output far-field beam profile. The particular shapes of the curves are induced by the spectral shift of the pump diode despite the internal grating [9].

significant change of the collimation between M2 and M3 mirrors when we vary the pump power. The gain medium is an Er:YAG single crystal fiber manufactured by Fibercryst with a doping concentration of 0.5%, a diameter of 750 μm, and a length of 30 mm mounted in an optimized water-cooled copper heat-sink holder. The pump light is provided by a fiber-coupled laser diode with a core diameter of 400 μm and a numerical aperture of 0.22, delivering up to 40 W at 1532 nm. Its spectrum is narrowed down to 1 nm by an internal distributed Bragg reflector (DBR) grating. The pump beam is imaged inside the crystal with two 50 mm focal lenses, leading to a pump spot diameter of 400 μm.

In the first cavity [Fig. 6(a)], a thin-film polarizing mirror is inserted together with a 100 μm thick etalon and an aperture (the combination is denoted as "TFP+ etalon + aperture" in the following). Laser emission can occur at 1617 or 1645 nm. The etalon is adjusted to select laser emission at 1617 nm. In the second cavity [Fig. 6(b)], the TFP, etalon, and aperture are replaced by the RGM alone (denoted as "RGM" in the following). The grating lines were oriented vertically (i.e., perpendicular to the plane of incidence), inducing a vertical TE polarization. The emission wavelength only occurs at 1617 nm according to the wavelength selectivity of the RGM at the given incidence angle of 24.18°.

Without the aperture, more than 2.2 W of output power was extracted with the first resonator setup with a low beam quality ($M^2 = 3.8$). To enhance the beam quality, we introduced an aperture with an estimated diameter of 600 μm inside the cavity. The M^2 factor decreased to 2.4 while the output power dropped to 1.6 W. When we reduced the pinhole diameter below 600 μm, the laser threshold rapidly became too high for the available pump power.

The RGM configuration exhibited a M^2 factor of 1.4 on the vertical axis and 1.6 on the horizontal axis, with an output power of 1.4 W (Fig. 7). Despite the lower output power, this represents a brightness increase by a factor of 6.3 and 2.5 for the cavities without and with an aperture, respectively. An outline of these results is provided in Table 1.

By integrating the measured reflectivity of the grating mirror around the peak over the estimated divergence of the laser beam, one can find the effective reflectivity of the RGM. The laser beam divergence of the setup with the RGM is estimated at 0.1°, leading to a reflectivity

of 92%. This low value explains the degraded CW performances of the cavity (Fig. 7).

We estimated the divergence of a potential laser beam with a M^2 factor of 3.8 (corresponding to the beam quality of the first laser without the aperture) to be 0.27° at position corresponding to the RGM. With the same method as above, this would lead to an effective reflectivity of 82%. This value is significantly lower than the RGM reflectivity calculated for a beam with a M^2 of 1.4. Hence, the angular selectivity of the RGM is used as a beam spatial filter

Moreover, incident rays with a large vertical AOI are not fully TE anymore according to the grating lines orientation of the RGM since it will correspond to a conical incidence. Therefore, the resulting reflectivity for TE polarization will be much lower, explaining the spatial filtering and the beam quality improvement on both axes and not only on the perpendicular axis.

The polarization of the emitted beam was measured using a polarization analyzer combined to a rotating half-wave plate. The output beams were TE polarized (vertical). Comparable degrees of linear polarization (DOLP) in the range of 95%–96% were obtained in both configurations. This polarization ratio can be related to depolarization losses of the Er:YAG single crystal fiber which were estimated to be around 2% in single pass.

An optical spectral analyzer was used to record the spectra of the emitted beams. A spectral bandwidth of 100 pm (FWHM) for the TFP + etalon configuration was measured, whereas it was 70 pm for the RGM configuration (Fig. 8). The latter is close to the resolution limit of our analyzer. This slightly better spectral selectivity results from the narrow peak in the reflectivity curve of the RGM shown in Fig. 2.

In conclusion, we have demonstrated for the first time, to the best of our knowledge, the use of a RGM

Table 1. Performances Outline of the Experimental Setups

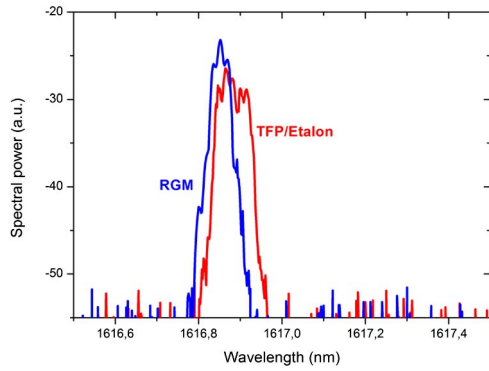| Setup	Power (W) P	$M^2_\parallel$	$M^2_\perp$	Brightness (a.u.) $P/(M^2_\parallel * M^2_\perp)$	Polarization Ratio (%)
TFP + Etalon	2.2	3.8	6.0	0.10	95
TFP + Etalon +Aperture	1.6	2.4	2.7	0.25	95
RGM	1.4	1.4	1.6	0.63	96

Fig. 8.   Measured spectra in both resonator configurations.

for emission control of an Er:YAG laser at 1617 nm. This unique optical component has a strong spatial, spectral, and polarization selectivity which can be achieved simultaneously and simplifies the resonator setups. It was shown that the brightness of the emitted beams at 1617 nm is improved by a factor of 2 thanks to the spatial (angular) selectivity of the RGM in comparison to standard resonator configuration based on the TFP + etalon + aperture combination. Moreover, a narrower spectral bandwidth is achieved with the RGM. Comparable DOLP are achieved for both experiments.

Further potential improvements can be made with an adequate resonator design to minimize the astigmatism and the ellipticity of the beam introduced by off-axis spherical mirrors. Furthermore, an improved RGM design with reduced propagation losses of the excited guided mode is expected to be possible according to our simulations and previous experimental investigations in different laser architectures (namely the thin-disk laser) [7]. In addition to complete laser emission control, RGM can also combine other functions such as a dichroic mirror or an output coupler. It may have great potential as a multifunctional mirror for laser cavities.

References
1. S. Li, T. Koscica, Y. Zhang, D. Li, and H.-L. Cui, Proc. SPIE **5995**, 59950Y (2005).
2. M. Rumpel, M. Haefner, T. Schoder, C. Pruss, A. Voss, W. Osten, M. A. Ahmed, and T. Graf, Opt. Lett. **37**, 1763 (2012).
3. V. A. Sychugov and A. V. Tishchenko, Quantum Electron. **10**, 186 (1980).
4. S. S. Wang and R. Magnusson, Appl. Opt. **32**, 2606 (1993).
5. D. Rosenblatt, A. Sharon, and A. A. Friesem, IEEE J. Quantum Electron. **33**, 2038 (1997).
6. M. M. Vogel, M. Rumpel, B. Weichelt, A. Voss, M. Haefner, C. Pruss, W. Osten, M. A. Ahmed, and T. Graf, Opt. Express **20**, 4024 (2012).
7. M. Rumpel, B. Dannecker, M. Moeller, C. Moormann, A. Voss, T. Graf, and M. A. Ahmed, Opt. Lett. **38**, 4766 (2013).
8. J. M. Bendickson, E. N. Glytsis, T. K. Gaylord, and D. L. Brundrett, J. Opt. Soc. Am. A **18**, 1912 (2001).
9. A. Aubourg, J. Didierjean, N. Aubry, F. Balembois, and P. Georges, Opt. Lett. **38**, 938 (2013).